Equilibrium Electroconvective Instability

I. Rubinstein* and B. Zaltzman†
Blaustein Institutes for Desert Research, Ben-Gurion University of the Negev, Sede Boqer Campus, Midreshet Ben-Gurion 84993, Israel

(Received 18 March 2014; published 16 March 2015)

Since its prediction 15 years ago, hydrodynamic instability in concentration polarization at a charge-selective interface has been attributed to nonequilibrium electro-osmosis related to the extended space charge which develops at the limiting current. This attribution had a double basis. On the one hand, it has been recognized that neither equilibrium electro-osmosis nor bulk electroconvection can yield instability for a perfectly charge-selective solid. On the other hand, it has been shown that nonequilibrium electro-osmosis can. The first theoretical studies in which electro-osmotic instability was predicted and analyzed employed the assumption of perfect charge selectivity for the sake of simplicity and so did the subsequent studies of various time-dependent and nonlinear features of electro-osmotic instability. In this Letter, we show that relaxing the assumption of perfect charge selectivity (tantamount to fixing the electrochemical potential of counterions in the solid) allows for the equilibrium electroconvective instability. In addition, we suggest a simple experimental test for determining the true, either equilibrium or nonequilibrium, origin of instability in concentration polarization.

DOI: 10.1103/PhysRevLett.114.114502 PACS numbers: 47.20.Ma, 47.57.jd

In recent years, electro-osmotic instability in concentration polarization at a charge-selective solid has attracted considerable interest on the part of both theoreticians and experimentalists [1–8]. Commonly, this instability has been attributed to nonequilibrium electro-osmosis (EO) related to the extended space charge [9–13], which develops in the course of concentration polarization at the limiting current [14]. One reason for this attribution was the realization that for a perfectly permselective (charge-selective) solid, [18], equilibrium EO cannot yield instability. Secondly, it has been shown that nonequilibrium EO can [19]. In the early studies, the assumption of perfect permselectivity was used for the sake of simplicity [9,13,19]. Subsequent studies of various time-dependent and nonlinear features of electro-osmotic instability [2,3,5,20] continued to do so, recognizing that the extended space charge lying at the basis of nonequilibrium EO is essentially identical for a perfect and nonperfect interface [21]. Here we report that relaxing the assumption of perfect permselectivity allows for equilibrium instability. Possible experimental tests for determining the equilibrium or nonequilibrium nature of hydrodynamic instability in concentration polarization in any particular setup are suggested.

dc ionic current in a binary electrolyte passing through a permselective interface (electrode, ion exchange membrane, micro-nano-channel junction) is a basic element of many electrochemical engineering or microfluidic processes, such as electrodeposition, electrodialysis, or protein preconcentration [22,23]. Such current passage is diffusion limited in the sense that it induces a decrease of electrolyte concentration towards the interface, the phenomenon known as the ionic concentration polarization. A common expression of it is a characteristic voltage-current curve with a segment in which the current nearly saturates at some plateau value, the limiting current, corresponding to the nearly vanishing interface concentration. This segment of the voltage-current curve is usually followed by a region of a relatively rapid increase of electric current with voltage—the so-called overlimiting conductance (OLC) regime. The mechanism of OLC remained unexplained for a long time. Only recently was it shown that in open systems OLC is due to the destruction of the diffusion layer by a microscale vortical flow which spontaneously develops as a result of instability of concentration polarization near the limiting current and provides an additional ionic transport mechanism yielding OLC [4,7,8,19,20,24,25]. This flow may be driven by the electric force acting upon both the space charge of a nanometers-thick interfacial electric double layer (EDL) and the residual space charge of the stoichiometrically electroneutral bulk. A sliplike fluid flow induced by the former is known as EO, whereas the flow induced by the latter is referred to as bulk electroconvection. There are two regimes of EO that correspond to different states of the EDL and are controlled by the nonequilibrium voltage drop (overvoltage) across it [13]: equilibrium EO and nonequilibrium EO, or EO of the second kind [4]. While both regimes result from the action of a tangential electric field upon the space charge of the EDL, the former relates to the charge of the equilibrium EDL, whereas the latter relates to the extended space charge of the nonequilibrium EDL that develops in the course of concentration polarization near the limiting current [10–12,14].

The theory of equilibrium EO at a permselective interface was developed by Dukhin and Derjaguin [26]. An essential component of this theory is accounting for polarization of the EDL by the applied tangential electric field, resulting in a lateral pressure drop in the double layer, owing to the lateral variation of the Maxwell stress. This yields for equilibrium EO slip velocity, instead of the common Helmholtz-Smoluchowski formula $u = -\zeta E$, the expression [13,14]

$$u = \zeta\left(\varphi_x + \frac{c_x}{c}\right) + \frac{c_x}{c}[4\ln 2 - 4\ln(e^{\zeta/2} + 1)]. \tag{1}$$

Here, φ is the dimensionless electric potential (scaled with the thermal potential, kT/e), c is the dimensionless electrolyte concentration (scaled with some typical concentration c_0), x is the dimensionless tangential coordinate (scaled with some typical macroscopic length, e.g., the membrane width), and ζ is the dimensionless electric potential drop between the interface and the outer edge of the EDL. The peculiarity of Eq. (1) is that, for an ideally permselective cation exchange membrane maintained at a fixed electric potential, the electrochemical potential of counterions in the membrane, $\ln c + \varphi = \text{const}$, is constant, and so it is, in equilibrium conditions, at the outer edge of the EDL. In other words, $\partial c/\partial x = -c\partial\varphi/\partial x$, and for $\zeta \to -\infty$, Eq. (1) yields

$$u = -4\ln 2\varphi_x. \tag{2}$$

Hydrodynamic stability of the quiescent concentration polarization with a limiting equilibrium EO slip condition (2) was studied by Zholkovskij *et al.* [18], who found that 1D concentration polarization was stable. So it was concluded that with a perfectly permselective interface no bulk electroconvective instability was feasible for a low molecular electrolyte [13,27]. In brief, the physical reason for this is that for an ideal interface, the stabilizing Donnan contribution to the electric potential perturbation, resulting from the concentration perturbation by the flow, dominates the corresponding destabilizing Ohmic contribution. Recognizing this balance has motivated the current reexamination of the role of perfect charge selectivity of the interface. (For a detailed discussion of bulk electroconvection versus equilibrium EO and the extent to which the two are equivalent, see Ref. [14].) On the other hand, it was shown that the nonequilibrium slip related to the extended space charge did yield instability [9,13,19]. This was the reason why, since its prediction in 1999 [9] till now, hydrodynamic instability in concentration polarization was attributed to nonequilibrium EO and was so studied [1–6,13].

It is the purpose of this Letter to show that any deviations from constancy of the electrochemical potential of counterions at the outer edge of EDL makes equilibrium instability possible. Nonconstancy of the counterionic electrochemical potential may result either from nonideal permselectivity of the interface (nonideally permselective nanoslot or ion-exchange membrane), addressed in this Letter, or from a finite rate of electrode reactions (e.g., in cathodic deposition). This Letter is structured as follows. We begin by formulating a three-layer model for a membrane flanked by two concentration polarized diffusion layers whose stability under no-slip (bulk electroconvection–no-slip setup) and equilibrium slip condition (1) (bulk electroconvection–EO setup) we analyze. Next, the results of a linear stability analysis in this model are presented, followed by the results of illustrative numerical simulations in the full nonlinear model.

Let us consider an infinite 2D cation-exchange membrane, $-\infty < x < \infty$, $0 < y < 1$, flanked by two diffusion layers, $-\infty < x < \infty$, $-L < y < 0$ and $-\infty < x < \infty$, $1 < y < 1 + L$, of a univalent electrolyte with concentration c_0 maintained at the outer boundary of diffusion layers [see Fig. 1(b)]. This three-layer system is modeled by the following boundary-value problem nondimensionalized in a natural manner [19]:

$$\frac{\partial c_\pm}{\partial t} = -\nabla \cdot \mathbf{j}_\pm, \tag{3}$$

$$\mathbf{j}_\pm = -c_\pm \nabla\mu_\pm + \mathrm{Pe}\mathbf{v}c_\pm, \qquad \mu_\pm = \ln c_\pm \pm \varphi. \tag{4}$$

Here, $c_\pm$ is the concentration of positive and negative ions and Pe is the material Peclet number [14,19]. Electroneutrality conditions in the enriched, $-L < y < 0$, and in the depleted, $1 < y < 1 + L$, diffusion layers and the membrane, $0 < y < 1$, read, respectively,

$$c_+ = c_- = C, \qquad -L < y < 0, \qquad 1 < y < 1 + L, \tag{5}$$

$$c_+ = c_- + N = C + \frac{N}{2}, \qquad 0 < y < 1. \tag{6}$$

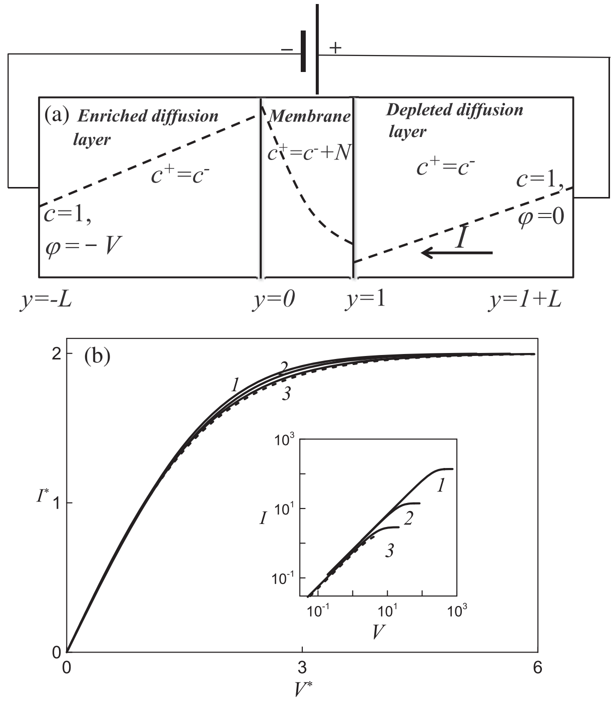

FIG. 1. (a) Scheme of three-layer setup, dashed lines are schematic plots of the average ionic concentration $C(y)$. (b) Scaled voltage-current dependence $L = 1$, (1) $N = 0.1$, (2) $N = 1$, (3) $N = 10$, dashed line corresponds to perfectly permselective interface. Inset: Same plots for unscaled voltage-current dependencies.

Here, N is the dimensionless fixed charge density in the membrane (scaled by ec_0) and $C = (c_+ + c_-)/2$ is the average ionic concentration. Let us neglect the fluid flow in the enriched diffusion layer and in the membrane, $\mathbf{v} = u\mathbf{i} + w\mathbf{j} \equiv 0$, $-L < y < 1$, and determine it in the depleted diffusion layer from the Stokes-continuity equations,

$$\nabla^2 \mathbf{v} - \nabla p + \nabla^2 \varphi \nabla \varphi = 0, \qquad \nabla \cdot \mathbf{v} = 0. \tag{7}$$

At the outer boundary of the depleted diffusion layer, we apply the reservoir conditions for velocity, $u_y(x, 1 + L) = 0$, $w(x, 1 + L) = 0$, along with prescribing the concentration and the electric potential at the outer edges of both diffusion layers:

$$C|_{y=-L,L+1} = 1, \qquad \varphi|_{y=-L} = -V, \qquad \varphi|_{y=L+1} = 0. \tag{8}$$

We complete the formulation by prescribing continuity of the ionic electrochemical potentials, $\mu_\pm$, and normal ionic fluxes through the membrane–solution interfaces, $y = 0, 1$ and the slip condition (1) at the membrane-depleted diffusion layer interface, $y = 1$. The main control parameters are the dimensionless voltage V, the dimensionless width of the diffusion layers L, and N. The latter is the measure of membrane charge selectivity, a perfect membrane corresponding to $N \gg 1$. For these conditions, the counterion concentration in the membrane equals N, which, combined with a fixed electric potential, amounts to fixing the electrochemical potential of counterions employed in the previous one-layer models [9,13,19]. In the three-layer model of this study, reducing N from infinity (perfect membrane) to a practical range, $N > 1$, amounts to allowing for lateral variations of the electrochemical potential of counterions in the membrane. The flow in the enriched compartment and the possible EO flow across the membrane are disregarded for simplicity, recognizing that hydrodynamic instability in concentration polarization is entirely due to large electric fields in the depleted diffusion layer.

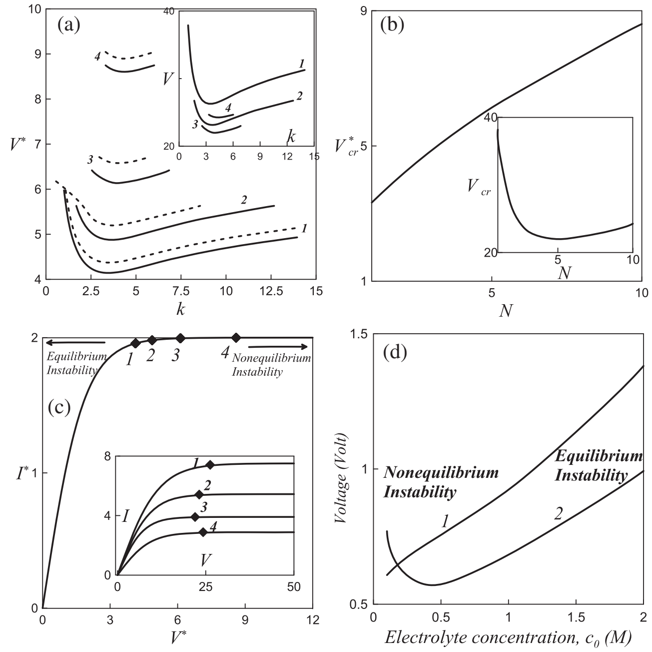

FIG. 2. (a) Neutral stability curves in scaled voltage V^*–wave number k plane (above the curve–instability), $L = 1$: $N = 2(1)$, $N = 3(2)$, $N = 5(3)$, $N = 10(4)$. Solid line stands for bulk electroconvection–EO setup and dashed line stands for bulk electroconvection–no-slip setup. Inset: Same for unscaled voltage V. (b) Scaled critical voltage for bulk electroconvection–EO setup $V^*_{\rm cr}$ versus N for $L = 1$. Inset: Same for $V_{\rm cr}$. (c) Instability threshold on the scaled V^*-I^* curve (bulk electroconvection–EO setup) for $L = 1$, $N = 2(1)$, $N = 3(2)$, $N = 5(3)$, $N = 10(4)$. Arrows mark variation of threshold with decreasing N (increasing bulk concentration in dimensional terms) for equilibrium bulk electroconvection–EO instability and nonequilibrium EO instability. Inset: Same four points on the V-I curves. (d) Instability threshold in the dimensional voltage-electrolyte concentration plane for nonequilibrium (1) and equilibrium (2) electroconvective instability. The membrane width is 100μ, $L = 1$, the concentration of fixed charges in the membrane is $4M$.

The quiescent 1D steady-state solution to the problem (1), (3)–(8) has been computed analytically in terms of Lambert functions. In Fig. 1(b) we present the computed voltage-current dependencies for various N (current density $\mathbf{I}$ is defined as $\mathbf{I} = \mathbf{j}^+ - \mathbf{j}^-$; in the figures, I is the normal component of $\mathbf{I}$ averaged over the interface). We note that whereas the voltage-current curves computed for different N

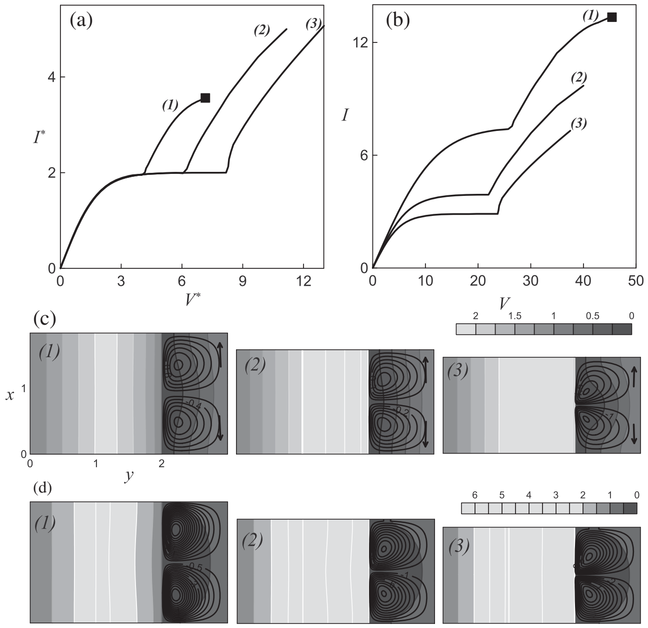

FIG. 3. (a) Steady-state V^*-I^* dependence $L = 1$: $N = 2(1)$, $N = 5(2)$, $N = 10(3)$. $N = 2$: black squares mark transition to time-dependent regime. (b) Same for unscaled voltage-current dependence. (c),(d) Concentration distribution (darker color corresponds to lower concentration) and flow streamlines computed for $L = 1$: $N = 2(1)$, $N = 5(2)$, $N = 10(3)$. (c) $V^* = 1.05V^*_{\rm cr}$ and (d) $V^* = 1.5V^*_{\rm cr}$. The rectangle corresponds to one spatial period of steady-state solution for critical wave number $k_{\rm cr}$, $0 < x < 2\pi/k_{\rm cr}$.

strongly differ due to the decrease of membrane permselectivity with the decrease of N [inset of Fig. 1(b)], upon a suitable scaling, the scaled $I^* - V^*$ curves collapse. Here, $I^* = I/I_0$, $V^* = V/V_0$, where I_0 is, e.g., one half of the limiting current $I_{\lim}$ and V_0 is the corresponding voltage.

The results of the linear stability analysis of the quiescent 1D steady state are presented in Fig. 2. The region above the neutral-stability curves plotted in Fig. 2(a) corresponds to instability. Whereas for unscaled voltage the unstable portion of the V-k plane shrinks exponentially upon the decrease of membrane permselectivity [inset of Fig. 2(a)], for scaled voltage the unstable portion of the voltage–wave number phase plane expands with decreasing N. The dependence of critical voltage on N is depicted in Fig. 2(b). Increase of the scaled critical voltage with N is a particular feature of equilibrium instability, potentially useful for the experimental identification of the OLC mechanism. To emphasize this, on the scaled voltage-current curve we mark four points corresponding to the onset of instability for a decreasing sequence of N (in dimensional terms, decreasing N is tantamount to increasing bulk solute concentration), Fig. 2(c), along with the corresponding plot in the unscaled V-I plane [inset of Fig. 2(c)]. We note that, whereas for a perfectly permselective membrane and its related nonequilibrium EO instability, the increase of bulk electrolyte concentration, resulting in the decrease of the dimensionless Debye length, yields an increase of the scaled threshold voltage [13], for equilibrium electroconvective instability, the increase of bulk concentration yields a decrease of N accompanied by a decrease of the scaled threshold voltage V^*, Fig. 2(c). As an additional illustration, in Fig. 2(d) we mark in the dimensional voltage-electrolyte concentration plane the parameter ranges in which, based on the linear stability analysis, each instability mechanism is expected to dominate (the nonequilibrium instability range is evaluated based on Ref. [13]). It is observed that, for a relatively high concentration of the fixed charges in the membrane, $4M$, the equilibrium instability is expected to set on prior to the nonequilibrium one for electrolyte concentrations above $0.1M$.

The linear stability analysis is complemented by numerical solution of nonlinear problem (1), (3)–(8) illustrated in Fig. 3. The transition to overlimiting conductance in Figs. 3(a) and 3(b) fits the results of the linear stability analysis. We note the supercritical character of the transition, as opposed to the subcritical one, accompanied by hysteresis in the nonequilibrium case for a realistic parameter range [8,20]. Black squares mark the transition to oscillations turning chaotic upon further increase of voltage for a poorly selective membrane, $N = 2$. The large separation between the onset of instability and the transition to unsteady regime is another "signature" of the equilibrium

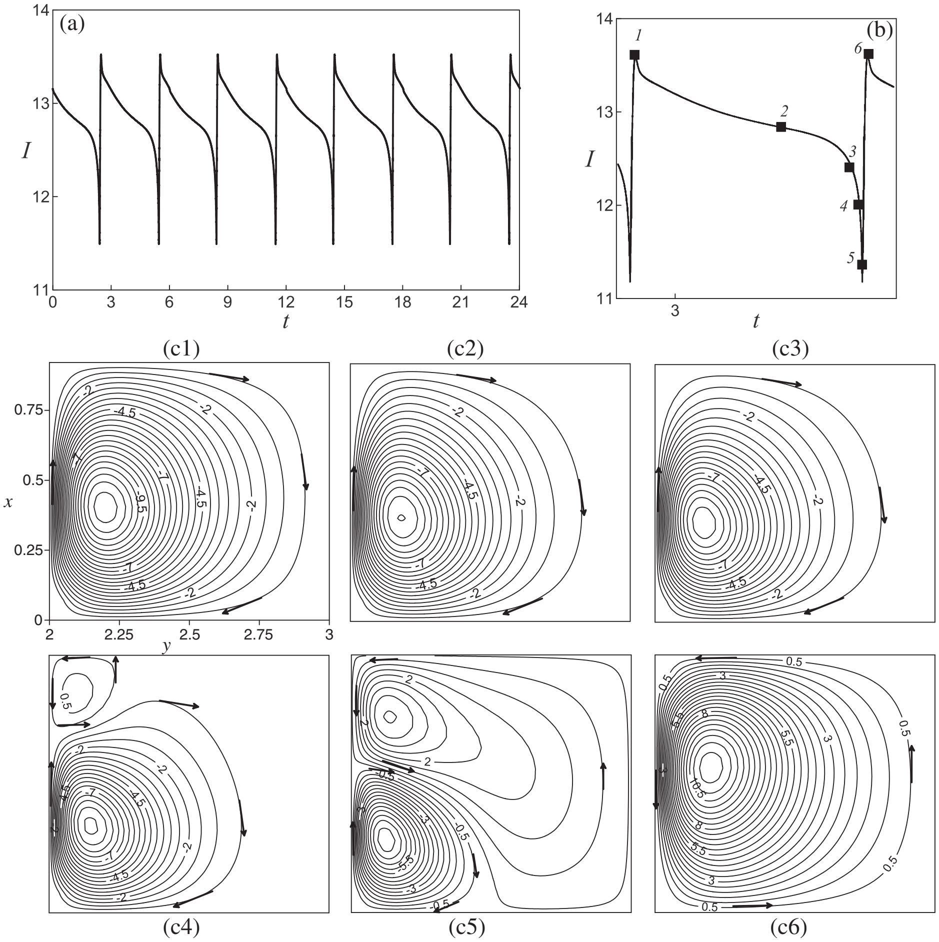

FIG. 4. (a) Periodic oscillations of I for $N = 2$, $L = 1$, $V = 44.78$. (b) One period of current oscillation. Six square points mark six time instants for which streamlines are drawn. (c) Streamlines for six time instants, drawn for half a spatial period: (c1)–(c3) correspond to points 1–3 in (b), increase of vortex asymmetry with time; (c4) corresponds to point 4 in (b), birth of an additional vortex in the upper left corner; (c5) corresponds to point 5 in (b), growth and eventual dominance of the new vortex; (c6) corresponds to point 6 in (b), disappearance of the original vortex with the resulting reversal of the sense of rotation.

instability as opposed to the nonequilibrium one. This unsteady regime is illustrated in Fig. 4, in which we depict the emerging periodic current oscillations and their underlying flow pattern for half a spatial period symmetry cell. The oscillation cycle emerging at the transition includes the phase of gradual growth of vortex asymmetry, Figs. 4(c1)–(c3), culminating in the birth of an additional pair of vortices near the interface stagnation point at the ascending side of the original vortices, Fig. 4(c). The growth of these emerging vortices, their eventual dominance, and disappearance of the original vortices yield a reversal of the sense of rotation in the symmetry cell, Fig. 4(c1) versus Fig. 4(c6).

To conclude, we point out that equilibrium bulk electroconvection–EO instability rather than its nonequilibrium counterpart may be accountable for the reported effects of depleted membrane surface modification by surfactants and polyelectrolyte deposition upon the onset of OLC [28]. Recently, this type of effect was analyzed in terms of nonequilibrium electro-osmotic instability [29].

The work was supported by the U.S.-Israel Binational Science Foundation (Grant No. 2010199).

---

[*] robinst@post.bgu.ac.il

[†] boris@bgu.ac.il

[1] R. Kwak, V. S. Pham, K. M. Lim, and J. Han, Phys. Rev. Lett. **110**, 114501 (2013).

[2] C. L. Druzgalski, M. B. Andersen, and A. Mani, Phys. Fluids **25**, 110804 (2013).

[3] E. A. Demekhin, N. V. Nikitin, and V. S. Shelistov, Phys. Fluids **25**, 122001 (2013).

[4] H. C. Chang, G. Yossifon, and E. A. Demekhin, Annu. Rev. Fluid Mech. **44**, 401 (2012).

[5] H. C. Chang, E. A. Demekhin, and V. S. Shelistov, Phys. Rev. E **86**, 046319 (2012).

[6] A. S. Khair, Phys. Fluids **23**, 072003 (2011).

[7] G. Yossifon and H. C. Chang, Phys. Rev. Lett. **101**, 254501 (2008).

[8] S. M. Rubinstein, G. Manukyan, A. Staicu, I. Rubinstein, B. Zaltzman, R. G. H. Lammertink, F. Mugele, and M. Wessling, Phys. Rev. Lett. **101**, 236101 (2008).

[9] I. Rubinstein and B. Zaltzman, in *Surface Chemistry and Electrochemistry of Membranes*, edited by T. S. Sorensen (Marcel Dekker, Inc., New York, 1999).

[10] W. H. Smyrl and J. Newman, Trans. Faraday Soc. **63**, 207 (1967).

[11] I. Rubinstein and L. Shtilman, J. Chem. Soc., Faraday Trans. 2 **75**, 231 (1979).

[12] M. Z. Bazant, K. T. Chu, and B. J. Bayly, SIAM J. Appl. Math. **65**, 1463 (2005).

[13] B. Zaltzman and I. Rubinstein, J. Fluid Mech. **579**, 173 (2007).

[14] See Supplemental Material at http://link.aps.org/supplemental/10.1103/PhysRevLett.114.114502, which includes Refs. [15–17], for details.

[15] V. G. Levich, *Physicochemical Hydrodynamics* (Prentice-Hall, Englewood Cliffs, NJ, 1962).

[16] B. M. Grafov and A. A. Chernenko, Dokl. Akad. Nauk SSSR **146**, 135 (1962); R. P. Buck, J. Electroanal. Chem. **46**, 1 (1973).

[17] A. V. Listovnichy, Sov. J. Electrochem. **25**, 1651 (1989); V. V. Nikonenko, V. I. Zabolotsky, and N. P. Gnusin, Sov. J. Electrochem. **25**, 262 (1989); K. T. Chu and M. Z. Bazant, SIAM J. Appl. Math. **65**, 1485 (2005).

[18] E. K. Zholkovskij, M. A. Vorotynsev, and E. Staude, J. Colloid Interface Sci. **181**, 28 (1996).

[19] I. Rubinstein and B. Zaltzman, Phys. Rev. E **62**, 2238 (2000); Math. Models Methods Appl. Sci. **11**, 263 (2001); I. Rubinstein, B. Zaltzman, J. Pretz, and C. Linder, Russ. J. Electrochem. 38, 853 (2002); I. Rubinstein and B. Zaltzman, Phys. Rev. E **68**, 032501 (2003).

[20] V. S. Pham, Z. Li, K. M. Lim, J. K. White, and J. Han, Phys. Rev. E **86**, 046310 (2012).

[21] J. A. Manzanares, W. D. Murphy, S. Mafe, and H. Reiss, J. Phys. Chem. **97**, 8524 (1993); I. Rubinstein and B. Zaltzman, Phys. Rev. E **81**, 061502 (2010).

[22] V. Fleury, J. N. Chazalviel, and M. Rosso, Phys. Rev. E **48**, 1279 (1993); J. M. Huth, H. L. Swinney, W. D. McCormick, A. Kuhn, and F. Argoul, Phys. Rev. E 51, 3444 (1995); M. Rosso, Electrochim. Acta **53**, 250 (2007); V. V. Nikonenko, N. D. Pismenskaya, E. I. Belova, P. Sistat, P. Huguet, G. Pourcelly, and C. Larchet, Adv. Colloid Interface Sci. **160**, 101 (2010); S. J. Kim, Y. C. Wang, J. H. Lee, H. Jang, and J. Han, Phys. Rev. Lett. **99**, 044501 (2007).

[23] M. K. Urtenov, A. M. Uzdenova, A. V. Kovalenko, V. V. Nikonenko, N. D. Pismenskaya, V. I. Vasileva, P. Sistat, and G. Pourcelly, J. Membr. Sci. **447**, 190 (2013).

[24] E. V. Dydek, B. Zaltzman, I. Rubinstein, D. S. Deng, A. Mani, and M. Z. Bazant, Phys. Rev. Lett. **107**, 118301 (2011).

[25] This pertains to nonconfined systems. Geometric confinement changes the mechanism of OLC in concentration polarization. In a very shallow microchannel (depth on a micron-submicron scale) facing a nanochannel (membrane), OLC is associated with the surface conduction effect. As the microchannel depth is increased to the tens of microns range, another mechanism—convection due to the EO flow along the charged channel walls—eventually takes over the surface conduction. For a dead-end channel sealed by an impermeable membrane, a pressure-driven flow develops to oppose the EO flow and results in the formation of two counterrotating vortices, which carry the concentrated solution to the membrane along the sidewalls and return the depleted solution along the channel axis. This circulation constitutes the dominant mechanism of OLC for the intermediate range of confinements. Upon further reduction of confinement, a transition to the hydrodynamic instability mechanism of OLC occurs.

[26] S. S. Dukhin and B. V. Derjaguin, *Electrophoresis* (Nauka, Moscow, 1976).

[27] B. D. Storey, B. Zaltzman, and I. Rubinstein, Phys. Rev. E **76**, 041501 (2007).

[28] M. Wessling, L. Garrigos Morcillo, and S. Abdu, Sci. Rep. **4**, 4294 (2014); N. P. Berezina, N. F. Fedorovitch, N. A. Kononenko, and E. N. Komkova, Russ. J. Electrochem. **29**, 1254 (1993); N. O. Berezina, V. A. Shaposhnik, D. V. Praslov, and O. P. Ivina, Russ. J. Phys. Chem. **64**, 2790 (1990).

[29] V. S. Shelistov, E. A. Demekhin, and G. S. Ganchenko, Phys. Rev. E **90**, 013001 (2014).